Received: 11 January 2023 | Accepted: 29 June 2023

DOI: 10.1097/HEP.0000000000000557

ORIGINAL ARTICLE

OPEN

Osteopontin characterizes bile duct–associated macrophages and correlates with liver fibrosis severity in primary sclerosing cholangitis

Kevin De Muynck[1,2] | Lander Heyerick[1,2] | Federico F. De Ponti[3,4] | Bart Vanderborght[2,5] | Tim Meese[6,7] | Sanne Van Campenhout[2,5] | Leen Baudonck[1] | Eva Gijbels[1,8] | Pedro M. Rodrigues[9,10,11] | Jesus M. Banales[9,10,11,12] | Mette Vesterhuus[13,14] | Trine Folseraas[13,15,16] | Charlotte L. Scott[3,4] | Mathieu Vinken[8] | Malaïka Van der Linden[17] | Anne Hoorens[17] | Jo Van Dorpe[17] | Sander Lefere[2,5] | Anja Geerts[2,5,18] | Filip Van Nieuwerburgh[6,7] | Xavier Verhelst[2,5,18] | Hans Van Vlierberghe[2,5,18] | Lindsey Devisscher[1,2]

[1]Department of Basic & Applied Medical Sciences, Gut-Liver Immunopharmacology Unit, Ghent University, Ghent, Belgium

[2]Liver Research Center Ghent, Ghent University, Ghent University Hospital, Ghent, Belgium

[3]Department of Biomedical Molecular Biology, Ghent University, Ghent, Belgium

[4]Laboratory of Myeloid Cell Biology in Tissue Damage and Inflammation, VIB-UGent Center for Inflammation Research, Ghent, Belgium

[5]Department of Internal Medicine and Paediatrics, Hepatology Research Unit, Ghent University, Ghent, Belgium

[6]Department of Pharmaceutics, Laboratory of Pharmaceutical Biotechnology, Ghent University, Ghent, Belgium

[7]NXTGNT, Ghent University, Ghent, Belgium

[8]Department of Pharmaceutical and Pharmacological Sciences, Vrije Universiteit Brussel (VUB), Brussels, Belgium

[9]Department of Liver and Gastrointestinal Diseases, Biodonostia Research Institute, Donostia University Hospital, University of the Basque Country (UPV-EHU), Donostia-San Sebastian, Spain

[10]CIBERehd, Instituto de Salud Carlos III (ISCIII), Madrid, Spain

[11]IKERBASQUE, Basque Foundation for Science, Bilbao, Spain

[12]Department of Biochemistry and Genetics, School of Sciences, University of Navarra, Pamplona, Spain

[13]Department of Transplantation Medicine, Division of Surgery, Inflammatory Medicine and Transplantation, Oslo University Hospital Rikshospitalet, Norwegian PSC Research Center, Oslo, Norway

[14]Department of Clinical Science, University of Bergen, Bergen, Norway

[15]Institute of Clinical Medicine, University of Oslo, Norway

[16]Research Institute of Internal Medicine, Division of Surgery, Inflammatory Medicine and Transplantation, Oslo University Hospital Rikshospitalet, Oslo, Norway

[17]Department of Pathology, Ghent University Hospital, Ghent, Belgium

[18]Department of Gastroenterology and Hepatology, Ghent University Hospital, Ghent, Belgium

Abbreviations: ALT, alanine transaminase; ALP, alkaline phosphatase; AST, aspartate aminotransferase; BMDMs, bone marrow–derived macrophages; CTRL, control; CBDL, common bile duct ligation; DDC, 3,5-diethoxycarbonyl-1,4-dihydrocollidine; DEG, differentially expressed genes; DSS, dextran sodium sulfate; HC, healthy control; IBD, inflammatory bowel disease; LPS, lipopolysaccharide; mAB, monoclonal antibody; MDR2, multidrug resistance P-glycoprotein 2; MF, macrophage; MoMF, monocyte-derived macrophage; ns, not significant; OPN/SPP1, osteopontin (human/mouse); PSC, primary sclerosing cholangitis; qPCR, quantitative PCR; TREM2, triggering receptor expressed on myeloid cells 2; UC, ulcerative colitis, WT, wild type.

Kevin De Muynck and Lander Heyerick shared authorship.

Supplemental Digital Content is available for this article. Direct URL citations are provided in the HTML and PDF versions of this article on the journal's website, www.hepjournal.com.

Correspondence
Lindsey Devisscher, Campus UZ Ghent, Corneel Heymanslaan 10, building B, Entrance 36, B-9000 Ghent, Belgium.
Email: Lindsey.Devisscher@ugent.be
.

Abstract

Background and Aims: Primary sclerosing cholangitis (PSC) is an immune-mediated cholestatic liver disease for which pharmacological treatment options are currently unavailable. PSC is strongly associated with colitis and a disruption of the gut-liver axis, and macrophages are involved in the pathogenesis of PSC. However, how gut-liver interactions and specific macrophage populations contribute to PSC is incompletely understood.

Approach and Results: We investigated the impact of cholestasis and colitis on the hepatic and colonic microenvironment, and performed an in-depth characterization of hepatic macrophage dynamics and function in models of concomitant cholangitis and colitis. Cholestasis-induced fibrosis was characterized by depletion of resident KCs, and enrichment of monocytes and monocyte-derived macrophages (MoMFs) in the liver. These MoMFs highly express triggering-receptor-expressed-on-myeloid-cells-2 (*Trem2*) and osteopontin (*Spp1*), markers assigned to hepatic bile duct-associated macrophages, and were enriched around the portal triad, which was confirmed in human PSC. Colitis induced monocyte/macrophage infiltration in the gut and liver, and enhanced cholestasis-induced MoMF-*Trem2* and *Spp1* upregulation, yet did not exacerbate liver fibrosis. Bone marrow chimeras showed that knockout of *Spp1* in infiltrated MoMFs exacerbates inflammation *in vivo* and *in vitro*, while monoclonal antibody–mediated neutralization of SPP1 conferred protection in experimental PSC. In human PSC patients, serum osteopontin levels are elevated compared to control, and significantly increased in advanced stage PSC and might serve as a prognostic biomarker for liver transplant-free survival.

Conclusions: Our data shed light on gut-liver axis perturbations and macrophage dynamics and function in PSC and highlight SPP1/OPN as a prognostic marker and future therapeutic target in PSC.

INTRODUCTION

Primary sclerosing cholangitis (PSC) is an immune-mediated, obstructive, cholestatic liver disease with a high risk of progressing to advanced hepatobiliary fibrosis and end-stage liver disease. Pharmacological treatments are currently lacking and render PSC as a major indication for liver transplantation.[1–3] To date, the pathogenesis of PSC is incompletely understood but alterations at the level of the gut-liver axis are proposed to be involved.[4–6] Markers of intestinal barrier leakage are increased in PSC and associated with poor prognosis,[7,8] and up to 80% of PSC patients have concomitant inflammatory bowel disease (IBD) of which the vast majority is diagnosed as colitis [PSC-ulcerative colitis (UC)].[1] Hepatic disease in PSC patients is distinctive from that observed in PSC-UC patients and PSC-UC patients show a milder intestinal phenotype compared to non-PSC-UC patients, but with increased risk of developing colorectal cancer.[1,9,10] Resulting from this, PSC is considered a prototypical disease in which the gut-liver axis is involved.[11,12] However, so far, in-depth understanding of the reciprocal effects of cholestatic and intestinal disease on the gut and the liver, and how this contributes to PSC is incompletely understood.

In addition, PSC is characterized by the development of multifocal fibroinflammatory bile duct strictures, and macrophages (MFs) are suggested to play an important role in this progression.[13–15] However, MFs represent a heterogeneous myeloid cell population, show a high level of plasticity, and shape their ontogeny-imprinted phenotype in response to the local microenvironment. As such, a multitude of functional polarization states in homeostasis, inflammation, wound healing, fibrogenesis, and resolution of disease have been attributed to these phagocytes.[16–18] Under homeostatic conditions, MFs play a pivotal role in

controlling tolerance to harmless microbes and molecules, while addressing adequate immune responses against pathogens that enter the gut and are drained toward the liver.[11] In the liver, tolerance is maintained by resident KCs that dominate the hepatic macrophage pool during steady-state conditions. However, our group and others have shown that KCs are depleted in experimental models for acute liver injury (acetaminophen),[19,20] NAFLD,[21–23] hepatocarcinogenesis[19,24,25,] and recently, cholestatic liver disease,[26] while monocytes and monocyte-derived macrophages (MoMFs) infiltrate the liver. During inflammation, monocytes infiltrate the liver and give rise to MoMF that contribute to inflammation, fibrosis, and resolution of disease depending on their phenotype. MFs accumulate in hepatic peribiliary regions in experimental sclerosing cholangitis and PSC patients,[14,27] and inhibition of monocyte recruitment was shown to reduce biliary injury and fibrosis in experimental sclerosing cholangitis.[14] However, inhibition of monocyte infiltration has recently been shown to aggravate liver fibrosis in experimental NASH.[28] Since macrophages shape their phenotype depending on environmental cues, the outcome of depletion strategies most likely depends on the stage of disease progression. Modulating the phenotype of distinct MF populations might be an interesting alternative, but requires in-depth knowledge of the functional properties of those cells at specific stages in disease progression.[29] From this, it is clear that in-depth characterization of the dynamics and functions of hepatic MF populations in PSC progression is required. The recent availability of specific liver MF markers now enables us to address this question.[21,26,28,30]

Here, we investigated the impact of gut-liver axis disruption on the liver and colonic microenvironment, with emphasis on the composition and phenotype of hepatic MFs, in mouse models for cholangitis-associated fibrosis and colitis, and extended our findings to human PSC. Our results hint toward osteopontin as a novel prognostic marker and therapeutic opportunity in PSC in the future.

METHODS

Patient cohorts and sampling

Serum samples were either directly collected from patients according to best clinical practice and processed following standard operation procedures, or retrieved from the Hiruz Biobank and/or the Gastroenterology/Hepatology Biobank (Ghent University Hospital, Ghent, Belgium). Additional samples were obtained by means of the Norwegian PSC Research Center (NoPSC) (Oslo, Norway) and the Biodonostia Research Institute (Donostia-San Sebastian, Spain).[31] Characteristics of included patients for serum analyses are summarized in Table 1. Paraffin-embedded liver biopsy samples or explant material were provided by the pathology department of Ghent University Hospital. Characteristics of included patients for immunohistochemistry are summarized in Table 2. All research was conducted in accordance with both the Declarations of Helsinki and Istanbul. Appropriate approval by the Medical Ethics Committee of the Ghent University Hospital was provided (Ethical Committee 2019/0611, Belgian registration number: B670201940078). A written informed consent was obtained from all subjects.

Experimental methods

Detailed methods are provided as Supplemental Materials and Methods, http://links.lww.com/HEP/H970 in the Supporting Information.

Statistical analysis

Statistical analysis and graphical representations were performed with GraphPad Prism 6 (GraphPad Software Inc., La Jolla, CA). Continuous variables are presented as mean ± SEM, unless indicated otherwise. Ordinal variables are presented as median ± interquartile range. Two group comparisons were performed using an unpaired *t* test with Welch correction or a Mann-Whitney *U* test. Multiple group comparisons were performed using a 1-way ANOVA with Tukey correction or a Kruskal-Wallis test with Dunn correction. Variables were tested for normality using D'Agostino-Pearson or Shapiro-Wilkes normality tests. To determine the prognostic value of serum sOPN and sTREM2 levels, a receiver operating curve analysis employing the area under the curve and Youden J statistic were calculated using R statistical software 4.2.3 (R Core Team (2023), Vienna, Austria). *p*-values are either shown or reported using an asterisks system (*$p < 0.05$, **$p < 0.01$, ***$p < 0.001$, ****$p < 0.0001$). $p < 0.05$ was considered statistically significant.

RESULTS

Resident KCs are reduced and MoMFs expand in the liver during fibrosing cholangitis development

To investigate the hepatic MF pool during obstructive cholangitis-associated fibrosis development, we used the common bile duct ligation (CBDL) model and analyzed the liver at 2, 4, and 6 weeks after surgery (Figure 1A and Supplemental Figure S1, http://links.lww.com/HEP/H990). In line with previous results from

TABLE 1 Patient characteristics (serum samples)

	PSC (n = 68)	IBD (n = 32)	HC (n = 29)
Average age (y) (min–max)	41 (17–75)	37 (19–62)	38 (24–62)
Male/female	49/19	21/11	20/9
PSC/PSC-IBD	22/46	—	—
Small duct/large duct/indeterminate	13/50/5	—	—
Overlap syndrome yes/no	22/46	—	—
Fibrosis (liver biopsy) (unknown/F0/F1/F2/F3/F4)	46/3/1/3/5/10	—	—
FIB-4	1.51 (0.25–10)	0.71 (0.20–1.61)	—
ALT (IU/L)	76.5 (8–275)	25.3 (9–85)	—
AST (IU/L)	56.9 (14–227)	21.3 (12–58)	—
ALP (IU/L)	225.8 (54–1013)	75.1 (41–178)	—
gGT (IU/L)	228.3 (10–1062)	36.1 (11–152)	—
CRP	6.1 (0.1–66.3)	3.8 (0.6–28.7)	—

Abbreviations: HC, healthy control; IBD, inflammatory bowel disease; PSC, primary sclerosing cholangitis.

our group[32,33] and others,[34] CBDL resulted in progressive hepatobiliary damage characterized by necrosis, ductular reaction, inflammation, and fibrosis. The inflammatory and fibrotic nature of the hepatic microenvironment was further corroborated at transcriptional level with increased expression already 2 weeks after surgery (Supplemental Figure 2, http://links.lww.com/HEP/H990). We then characterized the dynamics of the hepatic MF pool by means of flow cytometry analysis (Figure 1B). Compared to sham-operated mice, the livers of CBDL mice showed a reduction in numbers of $CD11b^{+}$, $F4/80^{+}$, $TIM4^{+}$ KCs at 4 weeks after surgery, while the numbers of $CD11b^{hi}$, $F4/80^{+}$, $TIM4^{-}$ MoMFs, $CD11b^{hi}$, $Ly6C^{hi}$, $Ly6G^{-}$ monocytes and $CD11b^{hi}$, $Ly6C^{hi}$, $Ly6G^{+}$ neutrophils were already increased 2 weeks after surgery (Figure 1C). Absolute cell numbers showed a gradual decrease of all these subsets during liver injury progression. Of note, colon tissue of CBDL mice showed infiltration of neutrophils, monocytes, and MoMFs, which gradually diminished during progressive injury. This cell infiltration was, however,

TABLE 2 Patient characteristics (liver tissue samples)

Patient	IBD	Age	Sex	Sampling date	Type	Fibrosis grade	ALT	AST	ALP	gGT	CRP
Healthy	—	unknown	unknown	—	Living donor	0	—	—	—	—	—
PSC 1	Yes	56	F	2012-09-28	Needle biopsy	0	67	60	586	381	9.3
PSC 2	Yes	48	F	2021-01-13	Needle biopsy	0	117	52	307	366	2.2
PSC 3	Yes	50	F	2009-12-18	Needle biopsy	1	22	18	82	52	0.1
PSC 4	No	36	M	2016-12-27	Needle biopsy	1	51	37	177	161	5.4
PSC 5	No	31	M	2016-01-13	Needle biopsy	2	37	66	85	25	0.6
PSC 6	Yes	27	M	2017-05-03	Needle biopsy	2	23	27	78	50	0.6
PSC 7	No	14	M	2016-01-15	Needle biopsy	3	270	190	456	426	0.6
PSC 8	Yes	34	M	2015-04-20	Needle biopsy	3	154	160	252	453	1
PSC 9	No	43	M	2018-03-26	Explant	4	52	76	237	273	9.7
PSC 10	No	36	M	2017-03-15	Explant	4	—	—	—	—	—
PSC 11	Unknown	Unknown	Unknown	2014-01-06	Explant	4	—	—	—	—	—

Abbreviations: ALT, alanine transaminase; ALP, alkaline phosphatase; AST, aspartate aminotransferase; IBD, inflammatory bowel disease.

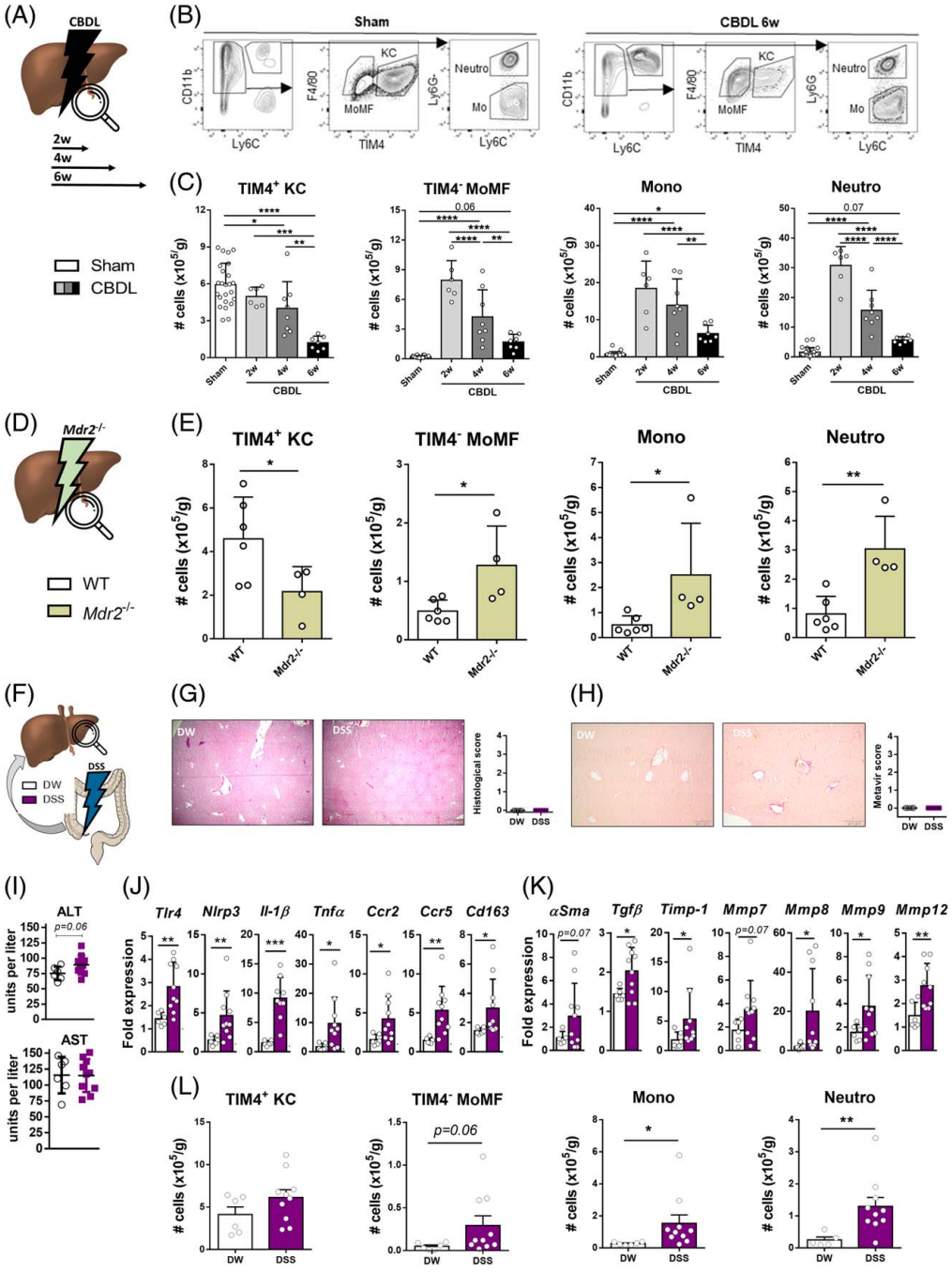

FIGURE 1 Hepatic myeloid cell composition during experimental fibrosing cholangitis or acute colitis. (A) Mice were subjected to CBDL (or Sham) operation and hepatic pathological features were analyzed 2-, 4-, and 6-week after surgery. (B) Gating strategy used to identify indicated myeloid cell populations (full gating strategy; see Supplemental Figure 1A, http://links.lww.com/HEP/H990). (C) Absolute cell quantification of isolated TIM4$^+$ KCs, MoMFs, Mono, and Neutro. Flow cytometry data are expressed as mean ± SD. N = 6–8 mice/group. A one-way ANOVA test was used to determine statistical significance. (D) Livers of 12-week-old *Mdr2*$^{-/-}$ mice or WT littermates were examined. (E) Absolute cell quantification of isolated myeloid cells in *Mdr2*$^{-/-}$ mice. A Student *t* test was used for statistical testing. (F) Mice received DSS at 2,5% w/v in drinking water for 7 days and hepatic pathological features were analyzed after 7 days. (G) Representative images of H&E-stained tissue slides, with scoring based on necrosis, ductular reaction, and inflammatory cell infiltration. Scale bars = 500 μm. (H) Representative images of picrosirius red stained tissue slides, with Metavir scoring. Scale bars = 200 μm. Histological scores are presented as median ± interquartile range. A Mann-Whitney test was used for statistical analysis. N = 6–10 mice/group. (I) Serum levels of alanine transaminase and aspartate aminotransferase. (J, K) mRNA expression of inflammation-related genes (J) and fibrosis-associated genes (K) in full liver tissue of DSS or DW mice. (L) Absolute cell quantification of isolated myeloid cells. Serum marker data, gene expression data, and flow cytometry data are represented as mean ± SD. N = 6–10 mice/group. A Student *t* test was used for statistical testing. *$p < 0.05$, **$p < 0.01$, ***$p < 0.001$, ****$p < 0.0001$, or *p*-values are shown. Each symbol represents one single mouse. Data are pooled from 2 to 3 independent experiments. Abbreviations: CBDL, common bile duct ligation; DSS, dextran sodium sulfate; DW, drinking water; H&E, hematoxylin & eosin; MoMF, monocyte-derived macrophage; Mono, monocyte; Neutro: neutrophil; WT, wild type.

not associated with an altered expression of inflammatory markers (Supplemental Figure S3, http://links.lww.com/HEP/H990).

To confirm the compositional changes observed in the hepatic myeloid cell pool during CBDL, we applied the same flow cytometry analysis on processed livers from 12-week-old multidrug resistance P-glycoprotein 2 (*Mdr2*$^{-/-}$) mice (Figure 1D). As expected, livers of *Mdr2*$^{-/-}$ mice, but not their wild-type (WT) littermates, showed hepatobiliary injury on histology (Supplemental Figure S4, http://links.lww.com/HEP/H990) and were characterized by a reduced number of TIM4^{+} KCs, while MoMFs, monocytes, and neutrophils were enriched (Figure 1E).

Myeloid cells infiltrate the liver during acute colitis but this does not exacerbate obstructive fibrosing cholangitis

Given the frequent concomitant presentation of PSC and colitis,[10] we subsequently investigated the impact of colonic barrier disruption and inflammation on the liver and myeloid cell composition, in health (Figure 1F) and during obstructive cholangitis. Dextran sodium sulfate (DSS)-induced colitis resulted in weight loss, colon shortening, and intestinal barrier degradation characterized by epithelial erosion, alterations in tight-junction gene expression, and colonic myeloid cell infiltration (Supplemental Figure S5, http://links.lww.com/HEP/H990). Liver weight remained stable (data not shown) and no histological liver damage or fibrosis was observed (Figure 1G,H), while serum levels of alanine transaminase tended to be elevated (Figure 1I). However, expression of inflammatory markers such as *Il1b, Tnfa*, and *Ccr2* and fibrosis-associated genes including *Tgfb*, *Timp1*, and various *Mmps* was upregulated in the livers of colitis mice (Figure 1J,K) and this coincided with increased numbers of neutrophils, monocytes, and MoMFs in the liver, while the TIM4^{+} KC pool remained stable (Figure 1L).

Next, we investigated how colitis alters obstructive fibrosing cholangitis progression. Colitis was induced at onset, during or at end-stage CBDL-induced liver injury and livers were analyzed at 6 weeks after surgery (Figure 2A). Administration of DSS at onset, during and at end-stage fibrosing cholangitis resulted in 23, 57, and 38% mortality, respectively, compared to 14% mortality in CBDL alone. Of note, end-stage CBDL mice were euthanized 7 days after DSS, whereas increased mortality in the other CBDL+DSS groups was observed between days 7 and 14 following start of DSS administration (Figure 2B). In all groups, administration of DSS was associated with weight loss and this was, remarkably, most pronounced in sham-operated mice (Figure 2C).

All CBDL groups showed comparable relative liver and spleen weight 6 weeks after surgery (Figure 2D). Serum levels of transaminases tended to be increased in end-stage CBDL-injured mice with active colitis compared to CBDL-only mice (Figure 2E). However, liver tissue sections showed no enhanced inflammation when DSS was administered at any time point during CBDL (Figure 2F), which was further corroborated with unaltered inflammatory gene expression levels (with exception for *Il1b*) (Figure 2G) and a similar number of neutrophils/Mos/MFs, compared to CBDL alone (Figure 2H). Metavir scoring of liver fibrosis showed that a higher number of mice exhibited F3 fibrosis in the end-stage CBDL+DSS group (Figure 2I). Semiquantitative determination of the collagen-positive area substantiated this trend (Figure 2J), although no differences were detected for alpha smooth muscle actin immunopositivity or hydroxyproline content (Figure 2K, L). In addition, hepatic mRNA expression of fibrotic markers showed no differences for *aSma*, *Tgfb*, and *Timp1*, while *Col1a* was downregulated and *Mmp8*, *10*, and *12* were upregulated in the end-stage CBDL+ DSS group (Figure 2M). Notably, colonic inflammation during end-stage CBDL was attenuated compared to colitis without pre-existing liver injury (Supplemental Figure 6, http://links.lww.com/HEP/H990).

To confirm that acute colitis does not aggravate advanced fibrosing cholangitis. we used a second combination model of cholestasis and colitis being the 3,5-diethoxycarbonyl-1,4-dihydrocollidine (DDC)-induced cholestatic liver injury and 2,4,6-trinitrobenzenesulfonic(TNBS)–induced colitis. DDC resulted in gradual weight loss and effectively induced liver injury characterized by inflammation, ductular reaction, and fibrosis whereas induction of 2,4,6-trinitrobenzenesulfonic–induced colitis in DDC fed mice tended to reduce hepatic inflammation and fibrosis (Supplemental Figure S7, http://links.lww.com/HEP/H990). Together these results show that acute colitis does not exacerbate fibrosing cholangitis.

Fibrosing cholangitis-associated MoMFs are characterized by osteopontin (*Spp1*) and triggering receptor on myeloid cells 2 (*Trem2*) expression which is enhanced during acute colitis

To further gain insight into the myeloid cell pool involved in the pathogenesis of cholangitis, colitis, and its combination, we isolated hepatic KCs, MoMFs, and Mos from mice during early (2w) and advanced (6w) CBDL-induced sclerosing cholangitis progression, with and without colitis, and control mice and performed mRNA-sequencing analyses on those cells. Principal component analysis clearly demonstrated segregation of the three myeloid populations from each other, as well as segregation of cells from CBDL mice from those of DSS

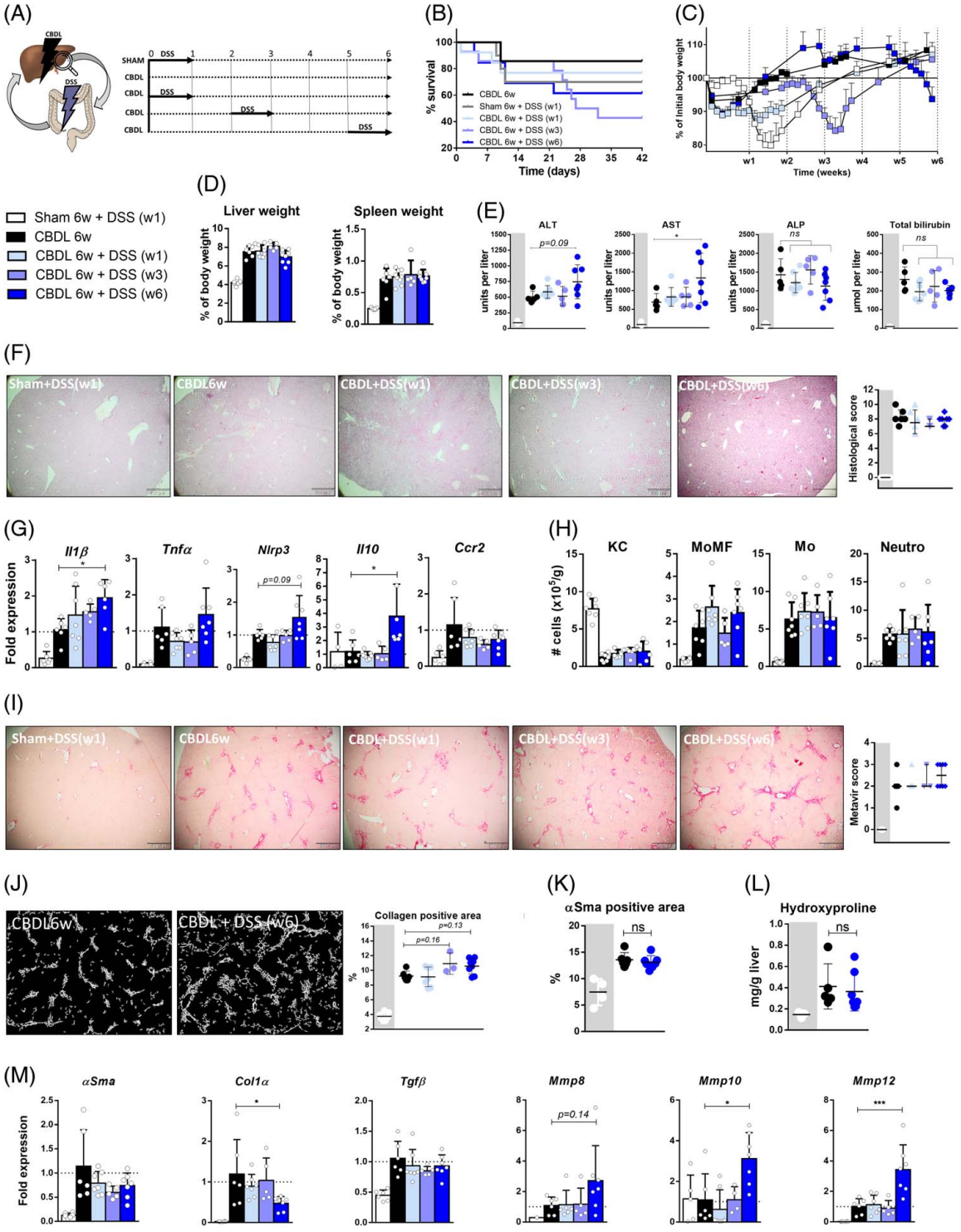

FIGURE 2 Hepatic alterations following induction of DSS-colitis during CBDL progression. (A) DSS was administered at onset, during or late-stage CBDL, and hepatic pathological features were examined compared to CBDL alone 6 weeks after surgery. (B) Kaplan-Meier survival curve during 6-week follow-up. (C) Percentage weight loss during 6 weeks. (D) Relative liver and spleen weight. (E) Serum biochemistry (alanine transaminase, aspartate aminotransferase, alkaline phosphatase, total bilirubin). (F) Representative images of H&E-stained tissue slides, with scoring based on inflammatory cell infiltration, ductular reaction, and necrosis. Scale bars = 500 μm. (G) mRNA expression of inflammation-related genes in full liver tissue. (H) Absolute cell quantification of hepatic myeloid cells. (I) Representative images of picrosirius red stained tissue slides with Metavir fibrosis scoring. (J) Semiquantitative analysis of fibrosis by means of picrosirius red stained area quantification (= collagen-positive area). N = 3–8 mice per group. Scale bars = 500 μm. (K) Semiquantitative analysis of aSMA positive area. (L) Hydroxyproline content. (M) mRNA expression of fibrosis-associated genes in full liver tissue. N = 3-8 mice/group. Data are pooled from 2 to 3 independent experiments. Serum biochemistry data, gene expression data, semiquantitative data, hydroxyproline content, and flow cytometry data are represented as mean ± SD. A 1-way ANOVA test was used to determine statistical significance. Histological scores are presented as median ± interquartile range with n = 3–8 mice/group. A Kruskal-Wallis test was used for statistical analysis. *$p < 0.05$, ***$p < 0.001$, or p-values are shown. Abbreviations: aSMA, alpha smooth muscle actin; CBDL, common bile duct ligation; DSS, dextran sodium sulfate; Mo, monocyte; MoMF, monocyte-derived macrophage; ns, not significant.

and control mice (Supplemental Figure S8, http://links.lww.com/HEP/H990). Differentially expressed genes (DEG) analysis of all CBDL mice grouped versus control mice revealed a specific fibrosing cholangitis-associated phenotype for each myeloid subset, which is distinct from the phenotypes induced by acute colitis in the corresponding cell types (Figure 3A,B). In response to CBDL, KCs showed enrichment of acute phase response genes and lysosomal activity genes, while monocytes became highly glycolytic and upregulated proinflammatory chemokines, including *Cxcl2*, *Cxcl3*, and *Spp1*. MoMFs prominently upregulated *Spp1*, *Trem2*, and *Gpnmb*, markers earlier described as signature genes for hepatic lipid-associated macrophages[23] (Figure 3A). Importantly, we confirmed the emergence of this lipid-associated macrophage phenotype in isolated MoMFs from livers of *Mdr2*$^{-/-}$ mice (Supplemental Figure S9A, http://links.lww.com/HEP/H990). Other upregulated MoMF markers included *Tgfbi*, *Il4ra,* and *Clec7a*, and functional annotation showed that all enriched DEGs were mostly associated with phagocytosis and extracellular matrix (ECM)-binding. Pairwise DEG analysis between CBDL2w and CBDL6w showed that the induced KC and monocyte phenotypes at onset remained stable over time (0 DEGs for both cell types). MoMFs showed a minimal response (28 DEGs total), with 23 downregulated genes, which remarkably included *Spp1, Trem2,* and *Vegfa.* In response to DSS, KCs upregulated apoptosis-related genes including *Birc5* and *Bak1*, while *Apoe* was strongly downregulated. Analysis of all upregulated genes in MoMFs showed a prominent increase in genes involved in inflammation, including *Tnfa*. Of note, monocytes upregulated a modest number of interferon-related genes (Figure 3B).

Pairwise DEG analysis between CBDL+DSS(w6) and CBDL6w resulted in 49, 285, and 30 total DEGs for KCs, MoMFs, and MOs, respectively, which suggests that MoMFs show the highest degree of plasticity during fibrosing cholangitis and colitis. Importantly, acute colitis at late-stage fibrosing cholangitis enhanced the lipid-associated macrophage phenotype, characterized by upregulation of, among others, *Spp1* and *Trem2* (Figure 3C). Pathway analysis suggested that many enriched genes in CBDL+DSS(w6) MoMFs were associated with phagocytosis, lysosomal activity, and extracellular matrix remodeling (data not shown).

We next mapped a set of inflammatory and fibrosis-associated genes onto all experimental groups per cell type (Figure 3D). *Il1b* expression was most prominently induced in hepatic MoMFs and MOs in CBDL2w and DSS, while *Tnfa* and *Il12b* expression were characteristic for DSS-associated liver MoMFs. *Cxcl1* and *Cxcl2* were highly expressed in MoMFs and MOs of CBDL2w. KCs specifically upregulated *Cxcl13* in response to DSS, but downregulated this chemokine in response to CBDL. *Tgfbi* and *Vegfa* expression were most prominently induced in MoMFs and MOs, but not KCs. In general, fibroinflammatory gene expression profiles differed per cell type and the induction of expression in either CBDL or DSS was most outspoken in MoMFs and MOs. Intercell comparison within each experimental group (Figure 3E) indeed showed that expression of *Il1b*, *Tnfa, and Tgfb* is lower in KCs compared to MoMFs in colitis and fibrosing cholangitis. Of note, mapping "KC signature genes" such as *Vsig4* and *Clec4f* corroborated our gating strategy, while mapping of *Spp1* and *Trem2* showed that, in general, *Spp1* was prominently differentially expressed in CBDL conditions. To confirm the MoMF versus KC CBDL-associated phenotype, we performed qPCR gene expression analysis of *Trem2* and *Spp1* on isolated TIM4^{+} KCs and MoMFs from livers of CBDL mice sacrificed 4 weeks after surgery. MoMFs indeed expressed higher levels of *Spp1*, but not *Trem2,* while *Il1b, Tnfa*, and *Tgfb* transcript levels were also higher (Figure 3F). MoMFs isolated from livers of 12-week-old *Mdr2*$^{-/-}$ mice showed a comparable phenotype (Supplemental Figure S9B, http://links.lww.com/HEP/H990). Additionally, we examined the expression levels of *Trem2* and *Spp1* in full liver tissue and found that both genes were upregulated in the liver following CBDL, but their expression was not further enhanced when colitis was induced during CBDL (Supplemental Figure 10, http://links.lww.com/HEP/H990).

Together, these results show that fibrosing cholangitis induces a dynamic shift in the liver macrophage pool with the emergence of fibrosis-associated MoMFs, typified by increased *Spp1* and *Trem2* expression.

Osteopontin expressing MoMFs accumulate near fibrotic regions in experimental and human PSC

Next, we wanted to gain insight into the spatial distribution of the identified MoMF subset and performed confocal microscopy on respective liver tissue of CBDL and control mice. Livers of control (Sham-operated) mice showed colocalization of F4/80 and CLEC4F outside of (peri)portal regions, corresponding to the topographical distribution of KCs. Within these portal regions SPP1 colocalized with EPCAM, denoting cholangiocytes/bile ducts, which are in proximity to DESMIN-rich spots, denoting portal fibroblasts (Figure 4A), together allowing localization of the portal triads. In contrast, portal areas of CBDL-injured mice were enriched with F4/80^{+} CLEC4F^{-} cells which colocalized with SPP1^{+} EPCAM^{-} spots. The DESMIN-positive area within the periportal regions was also increased in CBDL livers, corresponding to the increased periportal fibrosis observed in this model. Importantly, while F4/80 colocalized with CLEC4F, thus labeling *bona-fide* KCs, these areas covered interlobular nonfibrotic regions and did not colocalize

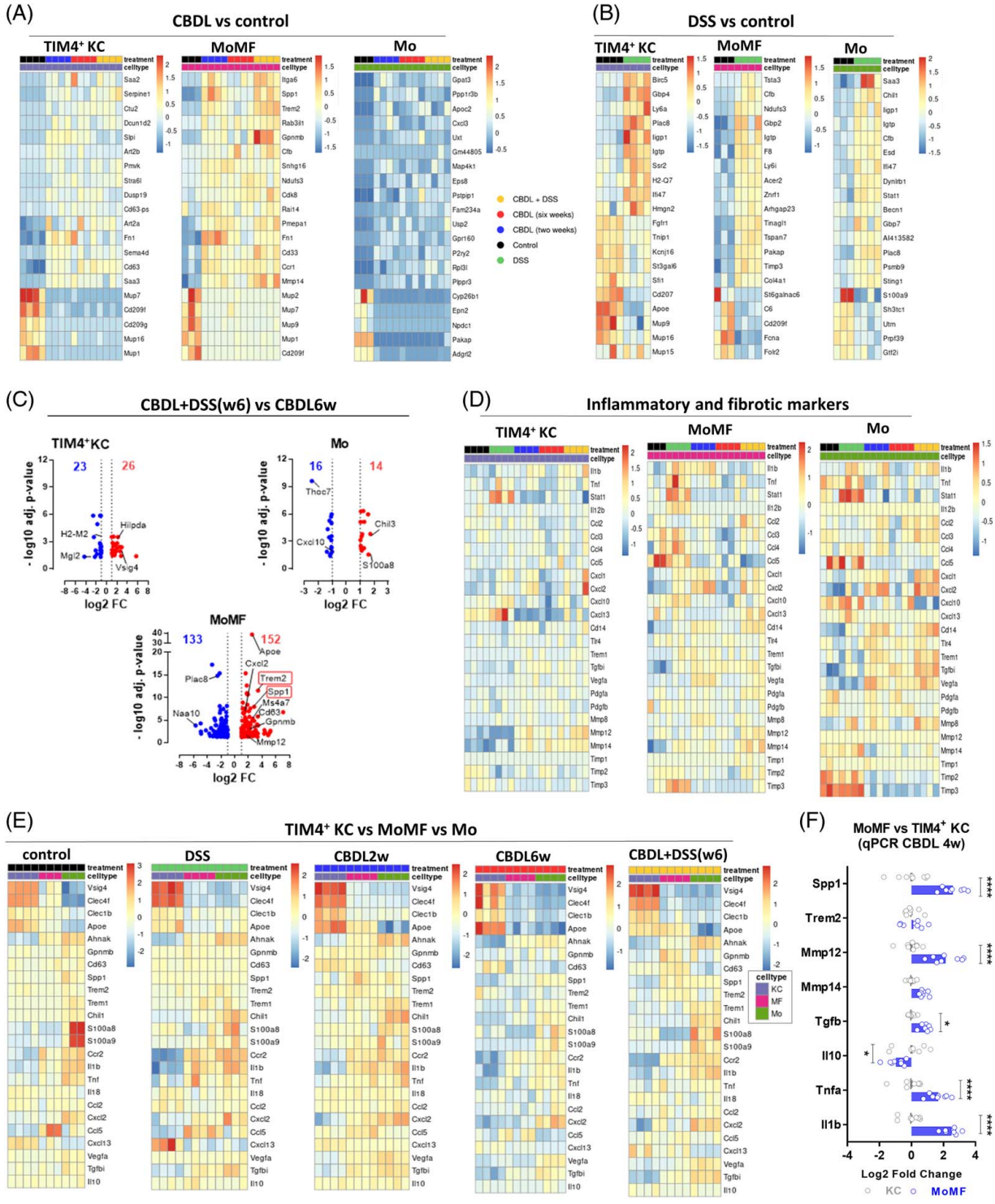

FIGURE 3 Transcriptional profiling of the liver myeloid cell pool identifies a *Trem2/Spp1*-expressing MoMF subset during CBDL. Heatmap showing top differentially expressed genes (DEGs) per cell type in all CBDL groups combined versus controls (A) or DSS versus controls (B). Group colors are indicated in the legend. (C) Volcano plot showing DEGs between CBDL6w and CBDL+ DSS(w6) with indicated numbers of upregulated (red) and downregulated (blue) genes. (D) Heatmap showing relative expression of fibroinflammatory markers per indicated cell type. (E) Intercell comparison showing mapping of subtype-specific signature genes and selected fibroinflammatory markers. All groups n = 4 mice/group, except MoMF and MO of the control group, where n = 3 mice/group. (F) qPCR gene expression analysis of selected markers in FACS-isolated KCs versus MoMFs from livers of CBDL 4w mice. Data presented as Log2 fold-change. A 2-way ANOVA with Bonferroni correction was used to test statistical significance. $*p < 0.05$, $****p < 0.0001$. N = 8 mice/group. Abbreviations: CBDL, common bile duct ligation; DSS, dextran sodium sulfate; MoMF, monocyte-derived macrophage; Mo, monocyte; qPCR, quantitative PCR.

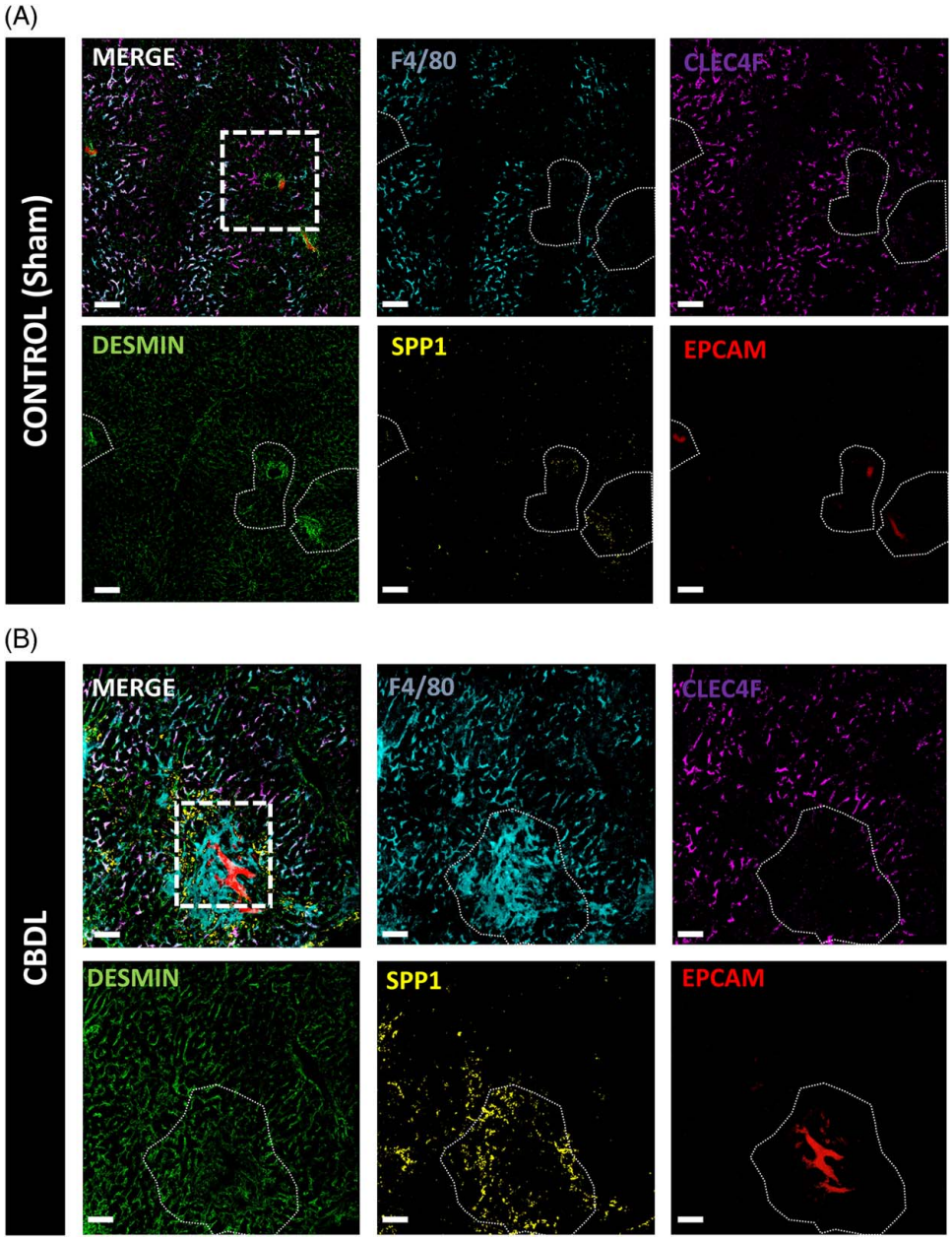

FIGURE 4 SPP1-expressing MoMFs accumulate near fibrotic regions in fibrosing cholangitis. Representative confocal microscopic images of liver sections from control (Sham) (A), CBDL6w (B), control (*Mdr2*$^{+/+}$ WT littermates) (C), *Mdr2*$^{-/-}$ (D), and DDC (E) mice stained with indicated antibodies. (A–E) Scale bars = 100 μm. Dotted circles represent portal areas. Dotted squares represent the insets grouped in a side-by-side manner in F. (F) Scale bars = 20 μm. Blue arrows mark SPP1^{+} EPCAM^{+} cholangiocytes. White arrows mark F4/80^{+} CLEC4F^{-}SPP1^{+} MoMFs. N = 2–4 mice per group. Abbreviations: CBDL, common bile duct ligation; DSS, dextran sodium sulfate; MoMF, monocyte-derived macrophage WT, wild type.

with SPP1 (Figure 4B). Similar to CBDL-injured livers, livers of *Mdr2*$^{-/-}$ mice, but not WT littermate controls, and DDC-diet fed mice showed periportal infiltration of F4/80^{+} CLEC4F^{-} cells (Figure 4C–E). At a higher magnification, a clear discrimination between F4/80^{+} CLEC4F^{-}SPP1^{+} and SPP1^{+} EPCAM^{+} was observed (Figure 4F).

We next evaluated the spatial distribution of OPN^{+} MFs in liver samples of PSC patients. Immunohistochemical stainings on serially cut liver sections showed accumulation of overlapping CD68^{+} and OPN^{+} spots in portal fibrous tissue regions in PSC patients, which was more pronounced in patients with advanced liver fibrosis (Figure 5).

Osteopontin suppresses macrophage proinflammatory function both *in vivo* and *in vitro*

To eludicate the role of *Spp1* in MFs, we performed bone marrow (BM) chimera experiments and subjected these

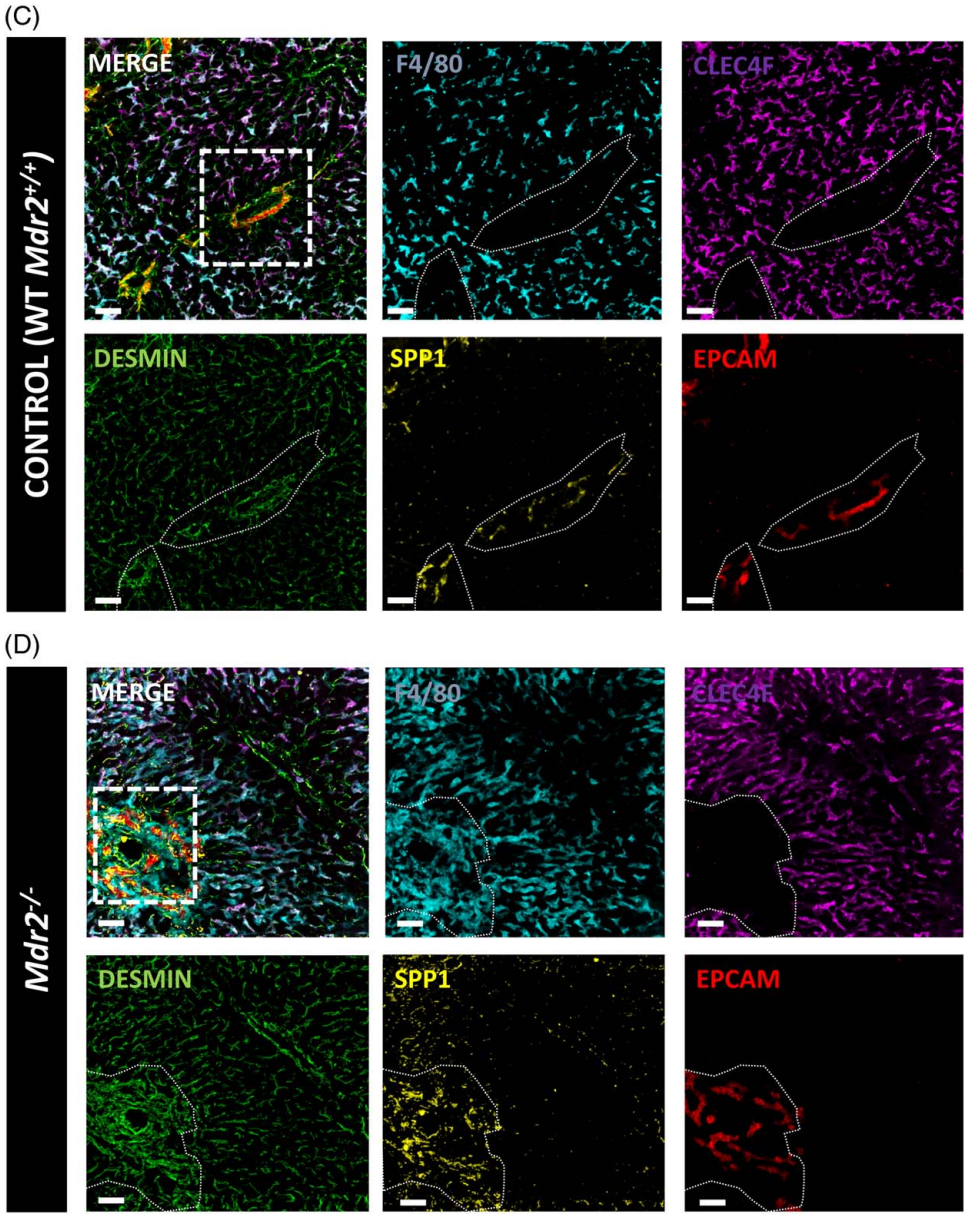

FIGURE 4 Continued

mice to CBDL (Figure 6A). At 2 weeks following CBDL, genotyping of BM isolated from *WT* acceptor mice showed the presence of a mutant band of 181 kb only in mice transplanted with *Spp1*$^{-/-}$ BM, thus confirming succesful engraftment (Figure 6B). Mortality was significantly higher in CBDL mice transplanted with *Spp1*$^{-/-}$ BM compared to those transplanted with *WT* BM (Figure 6C). Histological analysis of livers of mice that survived until experimental endpoint did not show differences between groups (Figure 6D, E). However, hematopoietic *Spp1* deficiency in CBDL mice was associated with increased induction of hepatic mRNA *Il1b*, *Timp1*, *Mmp12,* and *Ck19* expression (Figure 6F). Isolated MoMFs from CBDL-injured livers showed reduced induction of *Spp1* expression in mice transplanted with *Spp1*$^{-/-}$ BM compared to mice transplanted with *WT* BM. Similarly, but to a lesser extent, *Trem2* was less upregulated in *Spp1*$^{-/-}$ MoMFs following CBDL, although not significantly, while IL6 showed increased induction in MoMFs from *Spp1*$^{-/-}$ BM transplanted mice (Figure 6G).

In vitro, bone marrow-derived macrophages (BMDMs) of WT and *Spp1*$^{-/-}$ mice were exposed to supernatant of Hepa1-6 cells subjected to 3 repeated freeze-thaw cycles and lipopolysaccharide (LPS), either alone or sequentially administered (Figure 6H). In BMDMs of both genotypes, exposure to dying hepatoma supernatant alone did not induce inflammatory gene expression, but as expected, LPS stimulation did. LPS-induced inflammatory response was attenuated in BMDMs that were pre-exposed to supernatant of necrotic hepatoma cells. Importantly, in both conditions, LPS-induced secretion of

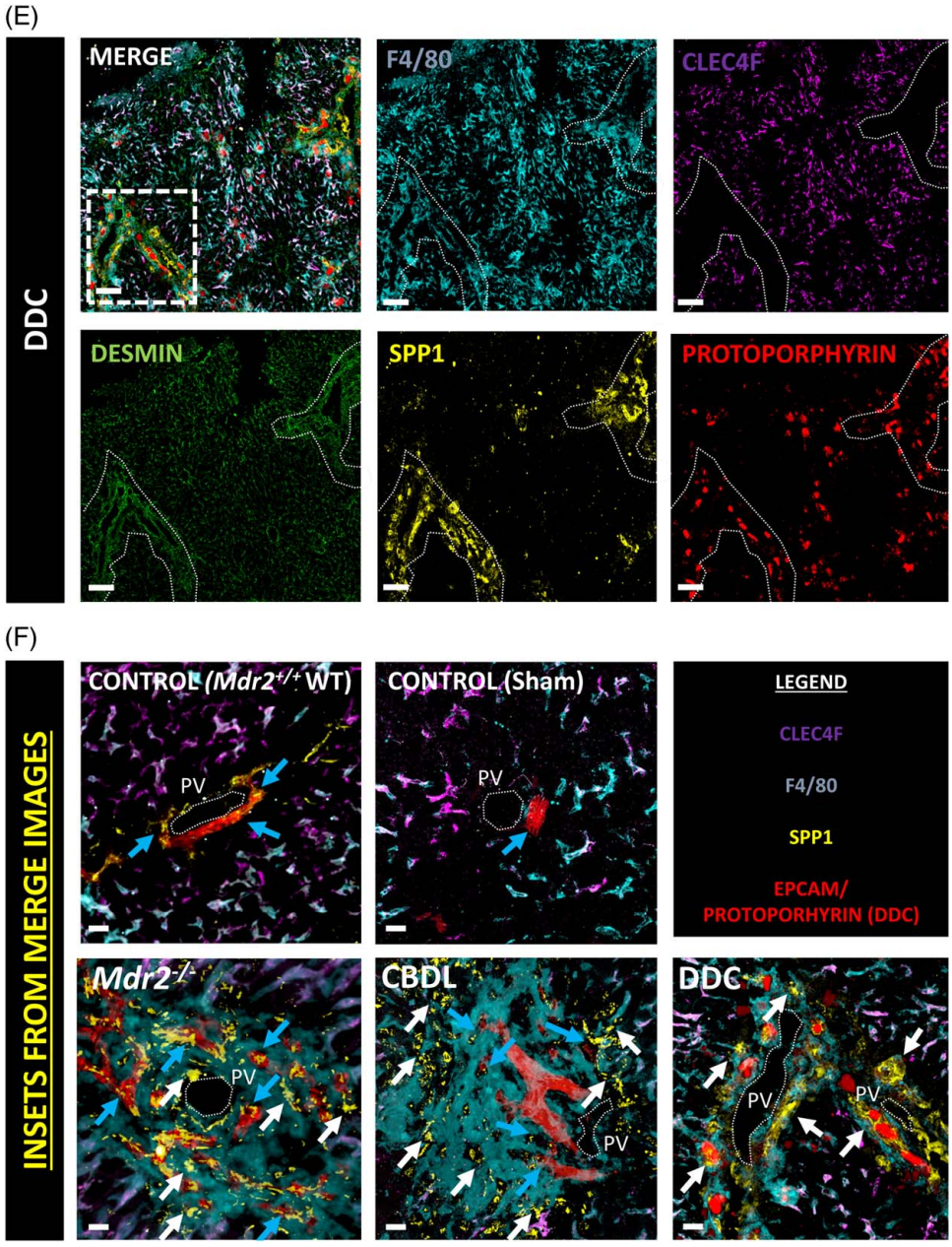

FIGURE 4 Continued

proinflammatory cytokines was higher in *Spp1*-deficient BMDMs compared to WT BMDMs (Figure 6I).

Together, these data show that hematopoietic osteopontin deficiency results in increased proinflammatoy capacity both *in vivo* and *in vitro*.

Serum sOPN levels are increased in PSC patients with advanced fibrosis and have prognostic potential

Given the identification and expansion of a *Spp1*$^{+}$ MoMF subset in our models and given that its soluble form has been proposed as a biomarker,[35,36] we evaluated sOPN levels in serum of transplant-naive PSC patients (Table 1). sOPN serum levels were significantly higher in PSC compared to IBD and healthy controls (Figure 7A). Stratification of these PSC patients according to fibrosis grade showed that the most prominent elevation occurs in PSC patients with F3-F4 fibrosis grade (Figure 7B). Our data also indicate that sOPN might serve as a prognostic biomarker for transplant-free survival in PSC patients (Figure 7C). sTREM2 levels followed these observations but did not correlate with liver fibrosis (Supplemental Figure 11, http://links.lww.com/HEP/H990). Serum SPP1 levels were also increased in the serum of CBDL, DDC-diet fed, and *Mdr2*$^{-/-}$ mice (Figure 7D).

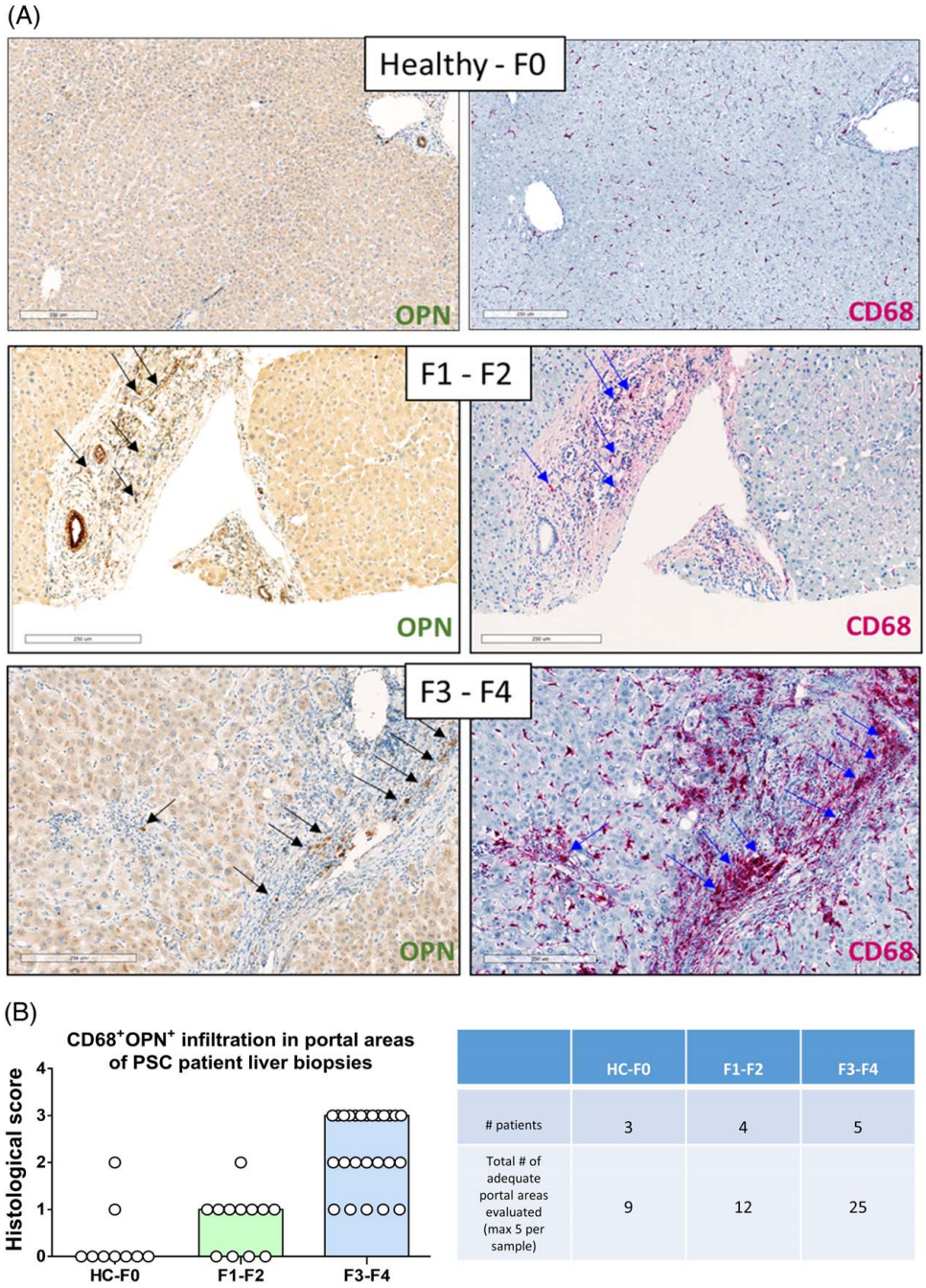

	HC-F0	F1-F2	F3-F4
# patients	3	4	5
Total # of adequate portal areas evaluated (max 5 per sample)	9	12	25

FIGURE 5 OPN and CD68 colocalize in livers of PSC patients. (A) Serially cut human liver sections of PSC patients with various fibrosis gradings stained for OPN (left panels) and CD68 (right panels). Scale bars = 250 μm. Black and blue arrows indicate where OPN and CD68 colocalize. (B) Histological score per adequate portal area. Bars represent median score. Each symbol represents a portal area. Number of included patients is indicated in the table to the right. Detailed patient characteristics are included in Table 2. Abbreviations: BM, bone marrow; CBDL, common bile duct ligation; CTRL, control; LPS, lipopolysaccharide; OPN, osteopontin; PSC, primary sclerosing cholangitis; WT, wild type.

Antibody-mediated neutralization of osteopontin ameliorates CBDL-induced liver injury

Osteopontin is a pleiotropic, versatile protein, and divergent roles of its intracellular versus secreted isoform (s) have been reported.[36] Therefore, and given the increased serum OPN/SPP1 levels, we next evaluated the effect of administering an anti-SPP1 monoclonal antibody (103D6)[37] in experimental PSC. Mice were subjected to CBDL and received treatment every other day (Figure 8A). CBDL-induced mice treated with anti-SPP1 antibodies showed less mortality (Figure 8B), lower serum alanine transaminase levels (Figure 8C), and less ductular reaction, necrosis and fibrosis on histology, and a tendency toward lower expression levels of inflammatory and fibrotic markers compared to IgG control–treated CBDL animals (Figure 8D–H).

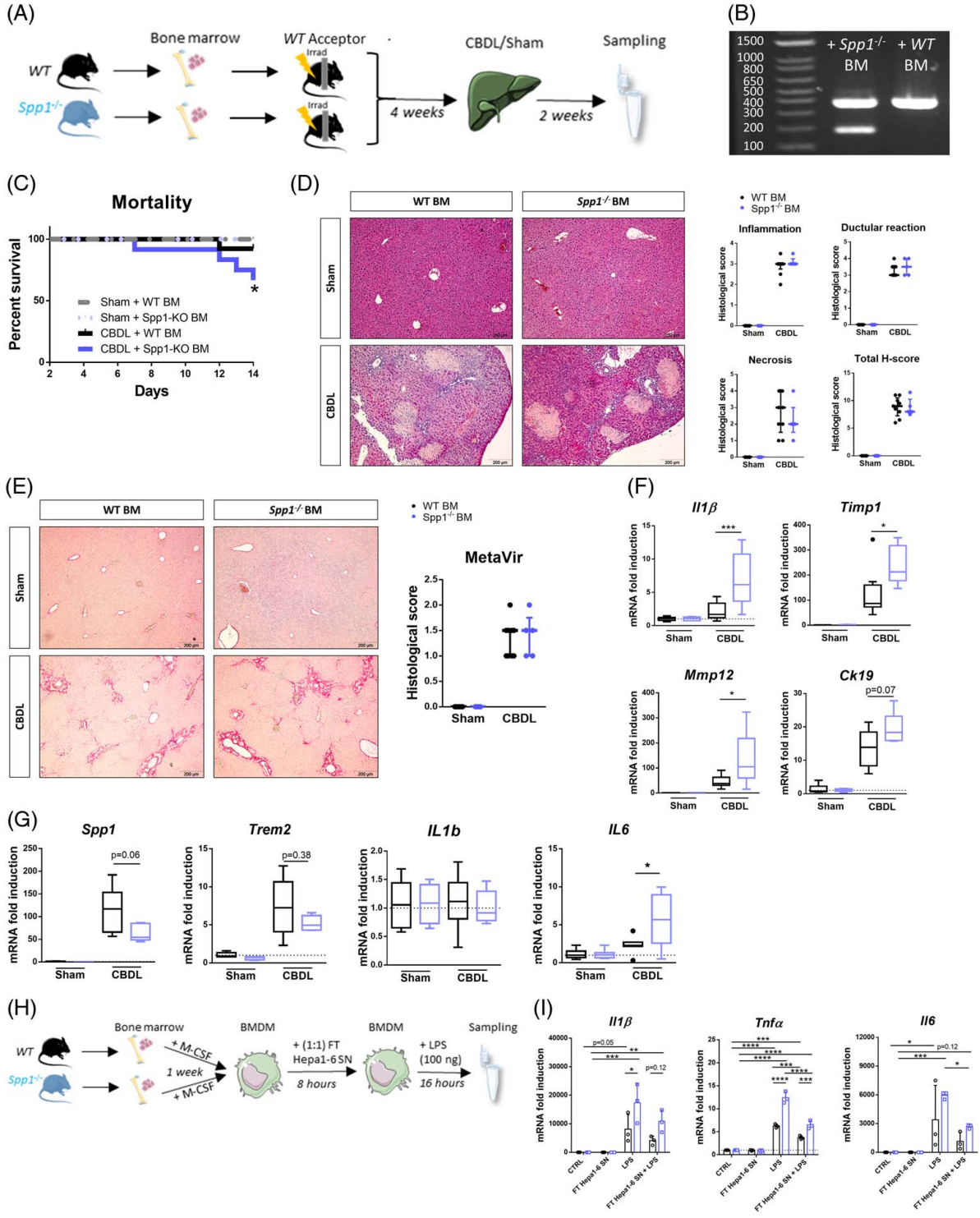

FIGURE 6 Osteopontin-deficiency enhances inflammation *in vivo* and *in vitro*. (A) Schematic setup of bone marrow transplant experiments. *Spp1*$^{-/-}$ or WT bone marrow was isolated and intravenously injected in irradiated WT acceptor mice which were subjected to either sham or CBDL surgery at 4 weeks post-transplantation. Gray rectangle represents a lead shield to protect the abdomen and liver. (B) Representative image of a DNA gel showing genotypes of isolated bone marrow from WT acceptor mice at experimental endpoint. (C) Mortality. Representative images of H&E-stained liver tissue (D) and scoring and Sirius Red stained liver tissue (E) and scoring. Data represent median + interquartile range. (F) Relative gene expression of liver injury-associated genes in full liver tissue. (G) Relative gene expression of *Spp1*, *Trem2*, *Il1b*, *and Il6* in isolated hepatic MoMFs. Data were pooled from 2 independent experiments and is presented as Tukey box plots with median and interquartile range. N = 5–9 mice per group. (H) Schematic setup of bone marrow–derived macrophage (BMDM) stimulation experiments. (I) Relative gene expression of inflammatory markers in *Spp1*$^{-/-}$ or WT BMDMs per indicated stimulation. Bars represent mean + SD. Three mice per genotype were used and stimulations were performed in triplicate. *$p < 0.05$, **$p < 0.01$, ***$p < 0.001$, ****$p < 0.0001$, or p-values are shown. 1:1 indicates the ratio of BMDMs to Hepa1-6 cells. Abbreviations: FT, freeze-thaw (3X); LPS, lipopolysaccharide; SN, supernatant.

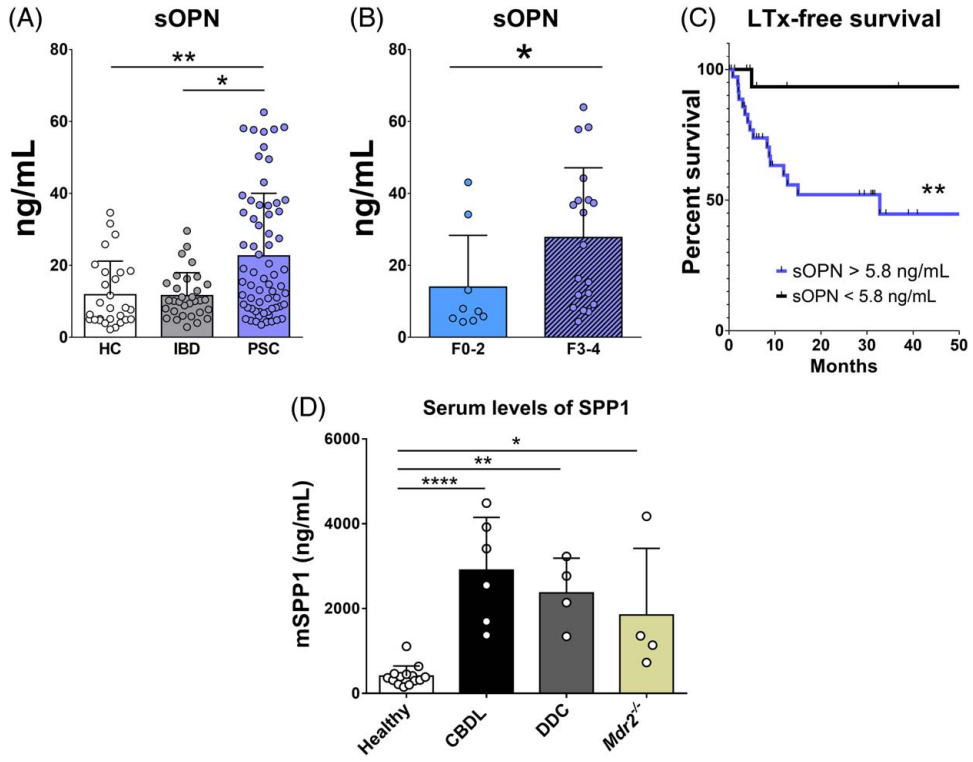

FIGURE 7 Serum sOPN is increased in PSC. (A) Soluble OPN (osteopontin) (sOPN) in serum of PSC or IBD patients versus HC. A 1-way ANOVA test with Tukey correction was used to determine statistical significance. (B) Stratification of sOPN according to liver fibrosis grade in a subcohort of PSC patients for which fibrosis grading data were available. A Mann-Whitney *U* test was used to determine statistical significance. (C) sOPN levels and transplant-free survival. Using Kaplan-Meier analysis and the log-rank test, liver transplant-free survival was compared between PSC patients that had sOPN concentrations above or below a determined optimal cutoff concentration (5.8 ng/mL). At this cutoff, an area under the ROC curve of 0.77 (95% CI, 0.62–0.91) was reached with a sensitivity and specificity of 0.95 and 0.69, respectively. (D) Soluble SPP1 (osteopontin) levels in serum of fibrosing cholangitis-injured mice versus healthy control mice. A 1-way ANOVA test with Tukey correction was used to determine statistical significance. Bars represent mean + SD. *$p < 0.05$, **$p < 0.01$, and ****$p < 0.0001$. Abbreviations: CBDL, common bile duct ligation; DDC, 3,5-diethoxycarbonyl-1,4-dihydrocollidine; HC, healthy control; IBD, inflammatory bowel disease; OPN, osteopontin; PSC, primary sclerosing cholangitis.

DISCUSSION

PSC is an idiopathic chronic liver disease for which no pharmacological treatment is available. In order to increase patients' treatment options, in-depth understanding of disease pathogenesis is required. A dysregulated gut-liver axis and immune response, in which macrophages play a central role, are involved in PSC; however, the exact modalities of gut-liver interactions and macrophage subsets and how these contribute to disease are unclear.[14,15]

As a first, we wanted to gain insight into the reciprocal effect of fibrosing cholangitis and colitis. Colitis resulted in increased hepatic fibroinflammatory gene expression and mild myeloid cell infiltration without inducing histopathological liver damage. Following fibrosing cholangitis, we observed an increase in mortality when colitis reached a peak in weight loss in all groups and when colitis was induced at more advanced liver injury. This corresponds to sepsis-associated death, similar to increased infection-related mortality observed in patients with cirrhosis.[38] In mice that survived colitis induction during early-stage or mid-stage fibrosing cholangitis, we did not observe lasting effects on the hepatic microenvironment compared to cholestatic mice without colitis. Colitis induction during advanced sclerosing cholangitis did not result in enhanced liver disease and fibrosis as evidenced by picrosirius red staining, aSMA immunopositivity and hydroxyproline content in the liver. Peng et al[39] previously showed that DSS aggravated hepatic fibrosis in the *Mdr2*$^{-/-}$ model, though only at their highest tested concentration (5%), which would have resulted in unacceptable increased mortality in our CBDL model. In turn, we observed an attenuation of colitis in mice with advanced fibrosing cholangitis, which corresponds to the milder UC phenotype in PSC patients and could serve as a model to further investigate concomitant PSC-UC presentation.

The identification of specific markers to identify distinct MF subsets in the liver has accelerated research into the role of macrophages in liver disease. By using TIM4 as KC-specific marker,[19,21,28,30] we show that TIM4^{+} KCs are depleted while Ly6C^{hi} MOs and Ly6C$^{-/lo}$TIM4^{-} MoMFs are enriched during fibrosing cholangitis. This is in line with the findings of Guicciardi et al in an acute BV6 and chronic *Mdr2*$^{-/-}$ cholestatic liver injury model based on CD11b, F4/80,

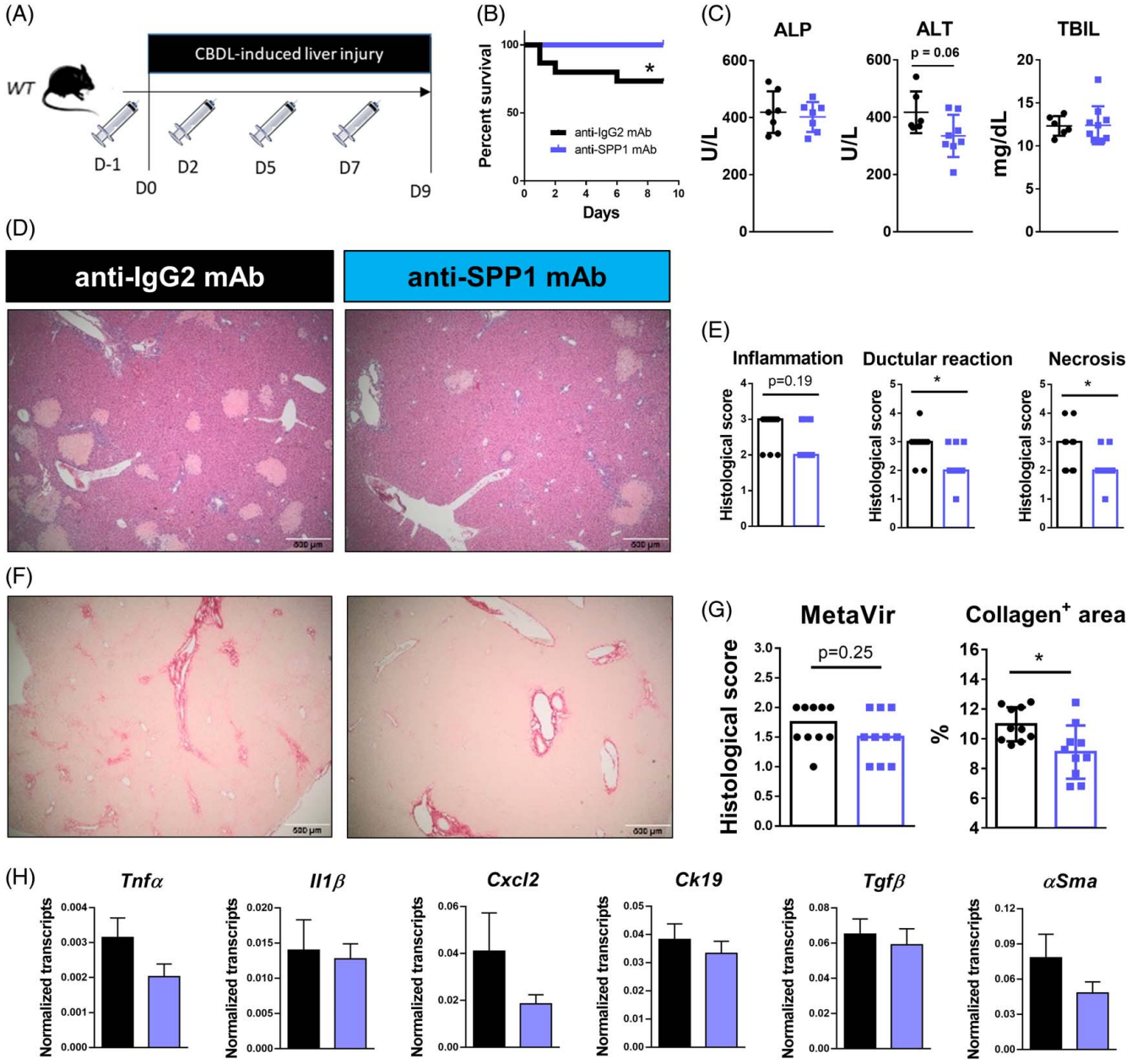

FIGURE 8 Neutralization of osteopontin ameliorates CBDL-induced liver injury. (A) Dosing scheme and experimental setup. (B) Mortality. (C) alkaline phosphatase, aspartate aminotransferase, and TBIL serum levels. (D) Representative images of H&E-stained liver tissue slides of anti-IgG2 or anti-OPN–treated CBDL-injured mice. (E) Histological scores for H&E. (F) Representative images of Sirius Red stained liver tissue slides. (G) MetaVir scoring and percentage collagen + area. Data presented as median + interquartile range (histo scores) or mean + SD (serum markers and collagen + area). (H) Normalized hepatic expression of indicated markers. A Mann-Whitney *U* test or a Student *t* test was used to determine statistical significance. N = 10 mice per group. $^*p < 0.05$. Abbreviations: CBDL, common bile duct ligation; mAB, monoclonal antibody; TBIL, total bilirubin; WT, wild type.

and Ly6C as surface markers.[14] Importantly, our results further substantiate that these compositional changes in the hepatic MF pool are a common event in response to various acute and chronic liver injuries.[19,21,23,28,40] Following fibrosing cholangitis induction, the most prominent transcriptional changes in isolated KCs, MoMFs and MOs were observed at onset (2 wk after CBDL). The fibrosing cholangitis-associated MoMF phenotype was characterized by a set of genes, including *Spp1, Trem2, Cd33*, *Fn1*, and *Gpnmb*, which closely resembles earlier described MF phenotypes associated with cirrhosis or NAFLD, being hepatic bile duct lipid-associated macrophages.[23,41–44] Topographically, we mapped these SPP1+ MoMFs to periductal/periportal desmin-rich areas in 3 mouse models for PSC and demonstrated that CLEC4F$^+$ KCs did not colocalize with SPP1. These data are in line with our and others' observation

that SPP1$^+$ MFs colocalize with fibrotic regions in NAFLD.[23,41,44] In PSC patients, we observed a similar spatial distribution of peribiliary enrichment of CD68$^+$ OPN$^+$ MFs, which correlated with fibrosis grade.

Osteopontin (SPP1/OPN) is a pleiotropic, highly versatile protein expressed by various cell types and has many potential proteoforms due to alternative splicing, a myriad of possible post-translational modifications and proteolytic processing.[36] As previous studies using whole-body *Spp1* deficiency reported conflicting outcomes in experimental PSC,[45–47] and we specifically wanted to target MoMFs, we here applied transplant experiments with *Spp1*-deficient BM. *Spp1* deficiency in MoMFs increased their inflammatory potential to LPS *in vitro* and resulted in enhanced liver inflammation *in vivo* following CBDL. These observations are in line with the reported role of intracellular SPP1 as a toll-like receptor signaling modulator.[48] In addition, a recent study in experimental NASH showed that myeloid-specific *Spp1* ablation aggravated liver inflammation, while myeloid-specific knock-in conferred protection, supporting our data.[49] Our data show that both *Spp1* and *Trem2* are upregulated in experimental PSC-associated MoMFs, but *Spp1* rather than *Trem2* was the most prominent differentially expressed marker when comparing MoMFs versus KCs. In line, Labiano et al recently showed that *Trem2* is predominantly upregulated in KCs (and HSCs) in livers of cholestatic mice and whole-body *Trem2* genetic ablation aggravated cholestatic liver injury.[50] Future studies investigating differential effects of hepatic stellate cell-, KC-, and MoMF-specific *Trem2* ablation or agonism in experimental PSC will be of interest.

Given that serum SPP1 levels were also increased in three PSC models, and SPP1 can be secreted from different cell types, we further explored the role of secreted/soluble SPP1 by using antibodies. Monoclonal antibody–mediated neutralization of SPP1 resulted in reduced CBDL-induced necrosis, ductular reaction, and fibrosis compared to control-treated animals, in line with recent data using the same approach in experimental NASH[51] and liver fibrosis.[52] SPP1 is also expressed by reactive cholangiocytes and stimulates ductular reaction.[53] Therefore, our neutralization approach can also block secreted SPP1 derived from other cellular (or even tissue) sources. Our data show a divergent role for SPP1, on the one hand intracellularly in MFs and on the other hand secreted extracellularly, which supports previous studies in this regard.[48,49,51–53] Further studies elucidating the more precise origin and role of secreted SPP1 in experimental PSC, including determining the relative levels of SPP1-specific isoforms and the balance between secreted and intracellular-related events, will be of interest. The tools to study this are currently being further developed.[36]

Finally, to underscore the translational value of our results, we show that sOPN levels are elevated, correlate with the degree of liver fibrosis and could serve as a prognostic marker in our cohort of PSC patients. Interestingly, sOPN is related to liver fibrosis under different chronic hepatopathological conditions such as ALD, NAFLD, hepatitis B, and C and can serve as a prognostic parameter for cirrhosis,[36] highlighting its significant role in liver disease.

In conclusion, our results shed light on alterations at the level of the gut-liver axis in the context of obstructive cholangitis and associated fibrosis and colitis, with specific emphasis on the heterogeneity of the hepatic MF pool. Our results show the manifestation of bile duct associated *Trem2*$^+$ /*Spp1*$^+$ MoMFs in cholangitis-associated fibrosis. We highlight osteopontin as prominent serum, hepatic, and macrophage marker with translational relevance, which opens the field for further investigation of its therapeutic potential in PSC.

DATA AVAILABILITY STATEMENT

All raw RNAseq data has been deposited to Gene Expression Omnibus (GSE183687).

AUTHOR CONTRIBUTIONS

Conceptualization: Kevin De Muynck and Lindsey Devisscher; experiments: Kevin De Muynck, Lander Heyerick, Federico F. De Ponti, Bart Vanderborght, Sanne Van Campenhout, Leen Baudonck, Eva Gijbels, and Malaïka Van der Linden; analyses: Kevin De Muynck, Lander Heyerick, Federico F. De Ponti, Bart Vanderborght, Tim Meese, Leen Baudonck, Eva Gijbels, Malaïka Van der Linden, Anne Hoorens, Jo Van Dorpe, Sander Lefere, Filip Van Nieuwerburgh, and Lindsey Devisscher; writing, Kevin De Muynck and Lindsey Devisscher; editing: Lindsey Devisscher; proofreading, Pedro M. Rodrigues, Jesus M. Banales, Mette Vesterhuus, Trine Folseraas, Charlotte L. Scott, Mathieu Vinken, Sander Lefere, Anja Geerts, Filip Van Nieuwerburgh, Xavier Verhelst, Hans Van Vlierberghe, and Lindsey Devisscher; funding acquisition, Lindsey Devisscher; supervision, Lindsey Devisscher.

ACKNOWLEDGMENTS

The authors thank Inge Van Colen, Els Van Deynse, Petra Van Wassenhove, Sophie Vermaut, Tim Pieters, Ran Rumes, Irem Kaya, and all personnel of the animal facility for the technical assistance. The authors also thank Elien Glorieus, Dr. Marie Truyens and Prof. Dr. Triana Lobatón-Ortega for the assistance in coordinating and securing IBD serum samples. For the use of scientific/medical images of cell types and organs the authors thank Servier Medical Art (https://smart.servier.com/). The authors also thank the Belgian Week of Gastroenterology, the Research Foundation Flanders – Strategic Research Network and the International PSC Study Group for the opportunity to present preliminary data related to this study.

FUNDING INFORMATION

This research is supported by Special Research Fund-Ghent University (BOF.STG. 2019.00.58.01-IV1) and Research Foundation Flanders (Fonds Wetenschappelijk Onderzoek, FWO) (G073723N). Bart Vanderborght was supported by Stand Up to Cancer- The Flemish Cancer Society (Kom op tegen Kanker, KOTK) (12726). Eva Gijbels was supported by FWO (1S47219N). Federico F. De Ponti is supported by FWO (1L2122N). Charlotte L. Scott is a Francqui Foundation Professor and supported by an ERC starting grant (MyeFattyLiver, 851908) and FWO project grants. Mathieu Vinken is supported by the FWO (G009514N and G010214N). Malaïka Van der Linden is supported by KOTK (001850372). Sander Lefere is supported by the FWO (12R0321N). Anja Geerts and Hans Van Vlierberghe are senior clinical FWO researchers (1805718N and 1801721N).

CONFLICTS OF INTEREST

Mette Vesterhuus is on the speakers' bureau for Intercept, Ely Lilly, and GE Healthineers. Xavier Verhelst consults, advises, is on the speakers' bureau, and received grants from Gilead. He received grants from AbbVie, Astellas, and Falk Pharma. The remaining authors have no conflicts to report.

ORCID

Kevin De Muynck https://orcid.org/0000–0003–3974–8473
Lander Heyerick https://orcid.org/0000–0002–5314–0707
Federico F. De Ponti https://orcid.org/0000–0003–0056–9099
Bart Vanderborght https://orcid.org/0000–0003–3964–6928
Tim Meese https://orcid.org/0000–0002–3307–9048
Sanne Van Campenhout https://orcid.org/0000–0001–9362–7475
Eva Gijbels https://orcid.org/0000–0002–7366–0769
Pedro M. Rodrigues https://orcid.org/0000–0001–6193–7436
Jesus M. Banales https://orcid.org/0000–0002–5224–2373
Mette Vesterhuus https://orcid.org/0000–0003–2994–2723
Trine Folseraas https://orcid.org/0000–0003–2011–1923
Charlotte L. Scott https://orcid.org/0000–0003–4914–6580
Mathieu Vinken https://orcid.org/0000–0001–5115–8893
Malaïka Van der Linden https://orcid.org/0000–0003–0249–908X
Anne Hoorens https://orcid.org/0000–0002–0736–2034
Jo Van Dorpe https://orcid.org/0000–0001–8175–2930
Sander Lefere https://orcid.org/0000–0001–5734–3467
Anja Geerts https://orcid.org/0000–0002–2218–9081
Filip Van Nieuwerburgh https://orcid.org/0000–0001–8815–5485
Xavier Verhelst https://orcid.org/0000–0002–2798–5415
Hans Van Vlierberghe https://orcid.org/0000–0003–0647–9238
Lindsey Devisscher https://orcid.org/0000–0003–4862–9580

REFERENCES

1. Lazaridis KN, LaRusso NF. Primary sclerosing cholangitis. N Engl J Med. 2016;375:1161–70.
2. Karlsen TH, Folseraas T, Thorburn D, Vesterhus M. Primary sclerosing cholangitis—a comprehensive review. J Hepatol. 2017;67:1298–323.
3. Dyson JK, Beuers U, Jones DEJ, Lohse AW, Hudson M. Primary sclerosing cholangitis. Lancet. 2018;391:2547–59.
4. Kummen M, Hov JR. The gut microbial influence on cholestatic liver disease. Liver Int. 2019;39:1186–96.
5. Liao L, Schneider KM, Galvez EJC, Frissen M, Marschall HU, Su H, et al. Intestinal dysbiosis augments liver disease progression via NLRP3 in a murine model of primary sclerosing cholangitis. Gut. 2019;68:1477–92.
6. Nakamoto N, Sasaki N, Aoki R, Miyamoto K, Suda W, Teratani T, et al. Gut pathobionts underlie intestinal barrier dysfunction and liver T helper 17 cell immune response in primary sclerosing cholangitis. Nat Microbiol. 2019;4:492–503.
7. Tornai T, Palyu E, Vitalis Z, Tornai I, Tornai D, Antal-Szalmas P, et al. Gut barrier failure biomarkers are associated with poor disease outcome in patients with primary sclerosing cholangitis. World J Gastroenterol. 2017;23:5412–21.
8. Dhillon AK, Kummen M, Troseid M, Akra S, Liaskou E, Moum B, et al. Circulating markers of gut barrier function associated with disease severity in primary sclerosing cholangitis. Liver Int. 2019;39:371–81.
9. Aranake-Chrisinger J, Dassopoulos T, Yan Y, Nalbantoglu I. Primary sclerosing cholangitis associated colitis: Characterization of clinical, histologic features, and their associations with liver transplantation. World J Gastroenterol. 2020;26:4126–39.
10. Tanaka A, Mertens JC. Ulcerative colitis with and without primary sclerosing cholangitis: Two different diseases ? Inflamm Intest Dis. 2016;1:9–14.
11. De Muynck K, Vanderborght B, Van Vlierberghe H, Devisscher L. The gut–liver axis in chronic liver disease: A macrophage perspective. Cells. 2021;10:2959.
12. Eksteen B. The gut-liver axis in primary sclerosing cholangitis. Clin Liver Dis. 2016;20:1–14.
13. Cameron RG, Blendis LM, Neuman MG. Accumulation of macrophages in primary sclerosing cholangitis. Clin Biochem. 2001;34:195–201.
14. Guicciardi ME, Trussoni CE, Krishnan A, Bronk SF, Lorenzo Pisarello MJ, O'Hara SP, et al. Macrophages contribute to the pathogenesis of sclerosing cholangitis in mice. J Hepatol. 2018;69:676–86.
15. Cadamuro M, Girardi N, Gores GJ, Strazzabosco M, Fabris L. The emerging role of macrophages in chronic cholangiopathies featuring biliary bibrosis: An attractive therapeutic target for orphan diseases. Front Med (Lausanne). 2020;7:115.
16. Wynn TA, Vannella KM. Macrophages in tissue repair, regeneration, and fibrosis. Immunity. 2016;44:450–62.

17. Gordon S, Plüddemann A. Tissue macrophages: heterogeneity and functions. BMC Biology. 2017;15:53.
18. Mowat AM, Scott CL, Bain CC. Barrier-tissue macrophages: Functional adaptation to environmental challenges. Nat Med. 2017;23:1258–70.
19. Lefere S, Degroote H, Van Vlierberghe H, Devisscher L. Unveiling the depletion of Kupffer cells in experimental hepatocarcinogenesis through liver macrophage subtype-specific markers. J Hepatol. 2019;71:631–3.
20. Devisscher L, Van Campenhout S, Lefere S, Raevens S, Tilleman L, Van Nieuwerburgh F, et al. Metallothioneins alter macrophage phenotype and represent novel therapeutic targets for acetaminophen-induced liver injury. J Leukoc Biol. 2021;111:123–33.
21. Devisscher L, Scott CL, Lefere S, Raevens S, Bogaerts E, Paridaens A, et al. Non-alcoholic steatohepatitis induces transient changes within the liver macrophage pool. Cell Immunol. 2017;322:74–83.
22. Lefere S, Puengel T, Hundertmark J, Penners C, Frank AK, Guillot A, et al. Differential effects of selective- and pan-PPAR agonists on experimental steatohepatitis and hepatic macrophages. J Hepatol. 2020;73:757–0.
23. Remmerie A, Martens L, Thoné T, Castoldi A, Seurinck R, Pavie B, et al. Osteopontin expression identifies a subset of recruited macrophages distinct from Kupffer cells in the fatty liver. Immunity. 2020;53:641–57.e614.
24. Vanderborght B, De Muynck K, Lefere S, Geerts A, Degroote H, Verhelst X, et al. Effect of isoform-specific HIF-1α and HIF-2α antisense oligonucleotides on tumorigenesis, inflammation and fibrosis in a hepatocellular carcinoma mouse model. Oncotarget. 2020;11:4504–20.
25. Degroote H, Lefere S, Vandierendonck A, Vanderborght B, Meese T, Van Nieuwerburgh F, et al. Characterization of the inflammatory microenvironment and hepatic macrophage subsets in experimental hepatocellular carcinoma models. Oncotarget. 2021;12:562–77.
26. De Muynck K, Vanderborght B, De Ponti FF, Gijbels E, Van Welden S, Guilliams M, et al. Kupffer cells contested as early drivers in the pathogenesis of primary sclerosing cholangitis. Am J Pathol. 2023;193:366–79.
27. Chen Y-Y, Arndtz K, Webb G, Corrigan M, Akiror S, Liaskou E, et al. Intrahepatic macrophage populations in the pathophysiology of primary sclerosing cholangitis. JHEP Rep. 2019;1:369–76.
28. Daemen S, Gainullina A, Kalugotla G, He L, Chan MM, Beals JW, et al. Dynamic shifts in the composition of resident and recruited macrophages influence tissue remodeling in NASH. Cell Rep. 2021;34:108626.
29. Tacke F. Targeting hepatic macrophages to treat liver diseases. J Hepatol. 2017;66:1300–2.
30. Scott CL, Zheng F, De Baetselier P, Martens L, Saeys Y, De Prijck S, et al. Bone marrow-derived monocytes give rise to self-renewing and fully differentiated Kupffer cells. Nature. Communications. 2016;7:10321.
31. Lapitz A, Azkargorta M, Milkiewicz P, Olaizola P, Zhuravleva E, Grimsrud MM, et al. Liquid biopsy-based protein biomarkers for risk prediction, early diagnosis, and prognostication of cholangiocarcinoma. J Hepatol. 2023;79:93–108.
32. Raevens S, Geerts A, Paridaens A, Lefere S, Verhelst X, Hoorens A, et al. Placental growth factor inhibition targets pulmonary angiogenesis and represents a therapy for hepatopulmonary syndrome in mice. Hepatology. 2018;68:634–51.
33. Costas-Rodríguez M, Van Campenhout S, Hastuti A, Devisscher L, Van Vlierberghe H, Vanhaecke F. Body distribution of stable copper isotopes during the progression of cholestatic liver disease induced by common bile duct ligation in mice. Metallomics. 2019;11:1093–3.
34. Abshagen K, König M, Hoppe A, Müller I, Ebert M, Weng H, et al. Pathobiochemical signatures of cholestatic liver disease in bile duct ligated mice. BMC Syst Biol. 2015;9:83.
35. Zhong L, Chen X-F. The emerging roles and therapeutic potential of soluble TREM2 in Alzheimer's disease. Front Aging Neurosci. 2019;11:328.
36. Song Z, Chen W, Athavale D, Ge X, Desert R, Das S, et al. Osteopontin takes center stage in chronic liver disease. Hepatology. 2021;73:1594–608.
37. Klement JD, Poschel DB, Lu C, Merting AD, Yang D, Redd PS, et al. Osteopontin blockade immunotherapy increases cytotoxic T lymphocyte lytic activity and suppresses colon tumor progression. Cancers (Basel). 2021;13:1006.
38. Arvaniti V, D'Amico G, Fede G, Manousou P, Tsochatzis E, Pleguezuelo M, et al. Infections in patients with cirrhosis increase mortality four-fold and should be used in determining prognosis. Gastroenterology. 2010;139:1246–56.e1245.
39. Peng Z-W, Rothweiler S, Wei G, Ikenaga N, Liu SB, Sverdlov DY, et al. The ectonucleotidase ENTPD1/CD39 limits biliary injury and fibrosis in mouse models of sclerosing cholangitis. Hepatol Commun. 2017;1:957–72.
40. Van Campenhout S, Tilleman L, Lefere S, Vandierendonck A, Raevens S, Verhelst X, et al. Myeloid-specific IRE1alpha deletion reduces tumour development in a diabetic, non-alcoholic steatohepatitis-induced hepatocellular carcinoma mouse model. Metabolism. 2020;107:154220.
41. Ramachandran P, Dobie R, Wilson-Kanamori JR, Dora EF, Henderson BEP, Luu NT, et al. Resolving the fibrotic niche of human liver cirrhosis at single-cell level. Nature. 2019;575:512–8.
42. Xiong XL, Kuang H, Ansari S, Liu TY, Gong JK, Wang S, et al. Landscape of intercellular crosstalk in healthy and NASH liver revealed by single-cell secretome gene analysis. Molecular Cell. 2019;75:644–64.
43. Seidman JS, Troutman TD, Sakai M, Gola A, Spann NJ, Bennett H, et al. Niche-specific reprogramming of epigenetic landscapes drives myeloid cell diversity in nonalcoholic steatohepatitis. Immunity. 2020;52:1057–74.e1057.
44. Guilliams M, Bonnardel J, Haest B, Vanderborght B, Wagner C, Remmerie A, et al. Spatial proteogenomics reveals distinct and evolutionarily conserved hepatic macrophage niches. Cell. 2022;185:379–96.e338.
45. Fickert P, Thueringer A, Moustafa T, Silbert D, Gumhold J, Tsybrovskyy O, et al. The role of osteopontin and tumor necrosis factor alpha receptor-1 in xenobiotic-induced cholangitis and biliary fibrosis in mice. Lab Invest. 2010;90:844–52.
46. Xiaodong W, Aritz L, Xiaodong G, Yongke L, Naoto K, Raquel U, et al. Osteopontin induces ductular reaction contributing to liver fibrosis. Gut. 2014;63:1805.
47. Yang M, Ramachandran A, Yan HM, Woolbright BL, Copple BL, Fickert P, et al. Osteopontin is an initial mediator of inflammation and liver injury during obstructive cholestasis after bile duct ligation in mice. Toxicol Lett. 2014;224:186–95.
48. Yang H, Ye X, Zhang X, Li X, Fu Q, Tang Z. Intracellular osteopontin negatively regulates toll-like receptor 4-mediated inflammatory response via regulating GSK3β and 4EBP1 phosphorylation. Cytokine. 2018;108:89–95.
49. Han H, Ge X, Babu Komakula SS, Desert R, Das S, Song Z, et al. Macrophage-derived osteopontin (SPP1) protects from non-alcoholic steatohepatitis. Gastroenterology. 2023;165:201–17.
50. Labiano I, Agirre-Lizaso A, Olaizola P, Echebarria A, Huici-Izagirre M, Olaizola I, et al. TREM-2 plays a protective role in cholestasis by acting as a negative regulator of inflammation. J Hepatol. 2022;77:991–1004.

51. Honda M, Kimura C, Uede T, Kon S. Neutralizing antibody against osteopontin attenuates non-alcoholic steatohepatitis in mice. J Cell Commun Signal. 2020;14:223–32.
52. Coombes JD, Swiderska-Syn M, Dollé L, Reid D, Eksteen B, Claridge L, et al. Osteopontin neutralisation abrogates the liver progenitor cell response and fibrogenesis in mice. Gut. 2015;64:1120–31.
53. Wang X, Lopategi A, Ge X, Lu Y, Kitamura N, Urtasun R, et al. Osteopontin induces ductular reaction contributing to liver fibrosis. Gut. 2014;63:1805–18.

How to cite this article: De Muynck K, Heyerick L, De Ponti FF, Vanderborght B, Meese T, Van Campenhout S, et al. Osteopontin characterizes bile duct–associated macrophages and correlates with liver fibrosis severity in primary sclerosing cholangitis. Hepatology. 2024;79:269–288. https://doi.org/10.1097/HEP.0000000000000557